Shape transformations of vesicles with intramembrane domains

Frank Jülicher[1,3] and Reinhard Lipowsky[1,2]
[1]*Institut für Festkörperforschung, Forschungszentrum Jülich, 52425 Jülich, Germany*
[2]*Max-Planck-Institut für Kolloid- und Grenzflächenforschung, Kantstraße 55, 14513 Teltow-Seehof, Germany*
[3]*Department of Physics, Simon Fraser University, Burnaby, British Columbia, Canada V5A 1S6*
(Received 1 August 1995)

Phase separation within the lipid bilayer of vesicles can lead to the formation of domains that affect the equilibrium shape of these vesicles. As a result of the competition between the bending energy of the bilayer and the line energy of the domain boundaries, the domains induce the formation of buds if their size is sufficiently large. This phenomenon of domain-induced budding is studied both for freely adapting and for fixed volume. The phase diagrams show that the constraint on the volume acts against the budding process, but will not, in general, suppress it. In many situations, domain-induced budding leads to limit shapes for which the bud consists of a closed sphere that is connected to the "mother" vesicle by an infinitesimal neck. This neck is characterized by a general and simple neck condition for the mean curvature of the membrane segments adjacent to the neck. Budding also occurs if the Gaussian bending energy is taken into account. The effect of the Gaussian curvature energy is to change the structure and the stability of those shapes that exhibit small necks.

PACS number(s): 87.22.−q, 82.70.−y, 64.60.−i

I. INTRODUCTION

Fluid lipid bilayer vesicles are spontaneously formed in aqueous solution. They can occur in a large variety of different shapes [1–7]. The conformational energy of a fluid membrane that is laterally homogeneous depends only on the shape of the vesicle characterized by the local curvatures of the surface [8]. The shape can thus be described as the shape of minimal bending energy taking into account global constraints on the surface area, the enclosed volume, and the topology of the surface [6,7,9–11].

The experimental observation of vesicle shapes reveals a variety of different families of shapes [2,3,12,13]. Most of them are of spherical topology, but tori and vesicles with higher topological genus have also been observed [14–16]. Shape transitions can be induced by changing control parameters such as temperature or osmotic conditions. A prominent example is the budding transition. In this case, the surface area of the membrane increases due to thermal expansion and the mirror symmetry of a prolate shape is broken in a discontinuous transition when the temperature is increased. A bud is formed, which is connected to the original vesicle by a small neck [2,3].

A lipid bilayer membrane in its fluid state has the properties of a two-dimensional liquid. If the bilayer consists of more than one species of molecules, it can either represent a homogeneous mixture or phase separate into two different fluid phases [17].

Biological membranes consist of many different types of lipid molecules and cholesterol [18,19]. Phase separation within mixtures of different lipid molecules has been observed experimentally for monolayer systems [20–22] and bilayers [19,23–26]. For lipid-cholesterol mixtures it has recently been shown that a phase separation into two fluid phases, one with a large and the other with a low cholesterol fraction, exists in the phase diagram of these mixtures [19,24–26]. Lipid-cholesterol mixtures have attracted a lot of interest since cholesterol plays an important role as a constituent of biological membranes [27,28].

If phase separation occurs within a membrane, the order parameter related to the demixing is an additional degree of freedom that is, in general, coupled to the shape of the vesicle. The shape therefore is not determined by the bending energy alone since the bilayer composition couples to the bilayer shape [17,29–41]. In fact, shape transformations induced by changes of the composition within the bilayer have been observed experimentally [13].

A domain embedded in the bilayer is bounded by an edge with a finite line tension σ. The line energy of a circular domain can in general be lowered by forming a bud connected by a small neck to the original vesicle [34,35,38]. If the edge of the domain is within the neck, the edge energy is essentially zero. The formation of a bud leads to an increase of the bending energy that is of the order of the bending rigidity κ, independent of the size of the bud. Budding will occur if the edge energy of the flat domain is of the same order of magnitude as the bending energy. The domain size at which both energies are comparable is given by the invagination length $\xi = \kappa/\sigma$, which shows that budding should in general occur if the domains are sufficiently large [34,35].

The present paper gives a systematic analysis of the equilibrium shapes of vesicles with intramembrane domains. A model for vesicles with domains is defined in Sec. II. Shape equations with appropriate matching conditions at the domain boundaries can be used to describe stationary shapes with axial symmetry. Equilibrium shapes that are obtained from these shape equations are discussed in Sec. III in terms of energy diagrams and phase diagrams for two different situations: (i) vesicles with no constraint on the enclosed volume and (ii) vesi-

cles with fixed volume. The role of the Gaussian curvature energy for vesicles with domains is studied in Sec. IV. Section V discusses the shape of a vesicle with a growing domain. The results of this work are discussed in Sec. VI and experiments are suggested by which one may observe shape changes induced by domains. Technical details are given in the Appendixes at the end of the paper. Some of these results have been reported previously in Ref. [38].

II. EQUILIBRIUM SHAPES OF VESICLES WITH FLUID DOMAINS

A. Free energy

A multicomponent vesicle consists of a mixture of different types of molecules that form a bilayer in aqueous solution. Here we will restrict ourselves to systems that undergo a phase separation into two *fluid* phases.

Within a lipid bilayer, phase separation can occur separately within both monolayers. We analyze two situations: (i) monolayer domains, which lead to an asymmetric bilayer and are thus characterized by a spontaneous curvature, and (ii) bilayer domains, for which the adjacent monolayers have the same composition. Thus we will ignore the possibility that there are two monolayer domains that will overlap only partially.

As long as the two types of molecules A and B mix within the membrane, the membrane is homogeneous and its surface area is fixed by the total number of molecules N_A+N_B. If one enters the coexistence region of the phase diagram, the membrane starts to separate into two coexisting phases. When the phase separation is completed, the membrane consists of two phases α and β. The total domain sizes $A^{(\alpha)}$ and $A^{(\beta)}$ are fixed by the constraint

$$A^{(\alpha)}\rho^{(\alpha)} + A^{(\beta)}\rho^{(\beta)} = N_A - N_B \quad , \tag{1}$$

where $\rho = \rho_A - \rho_B$ is the density difference and ρ_A, ρ_B are the number densities per unit area of the molecules of types A and B within the membrane.

The total energy of the vesicle can be expressed as

$$F = F_m + F_b + F_G \quad , \tag{2}$$

where F_b and F_G are the normal and the Gaussian bending energy, respectively [8]. The contribution

$$F_m \equiv A^{(\alpha)} f^{(\alpha)} + A^{(\beta)} f^{(\beta)} + F_l \tag{3}$$

denotes the free energy of the binary mixture. Here $f^{(\alpha)}$ and $f^{(\beta)}$ are the free energy densities of the two coexisting phases and

$$F_l = \sigma \int_{\partial\alpha} dl \tag{4}$$

is the energy of the domain boundary with line tension σ, which involves the integral along the boundaries $\partial\alpha$ of the α domains.

The bending energies F_b and F_G of a phase separated vesicle can be written as

$$F_b \equiv \frac{\kappa^{(\alpha)}}{2} \int_\alpha dA (C_1 + C_2 - C_0^{(\alpha)})^2 + \frac{\kappa^{(\beta)}}{2} \int_\beta dA (C_1 + C_2 - C_0^{(\beta)})^2 \tag{5}$$

and

$$F_G \equiv \kappa_G^{(\alpha)} \int_\alpha dA\, C_1 C_2 + \kappa_G^{(\beta)} \int_\beta dA\, C_1 C_2 \quad . \tag{6}$$

Here $\frac{1}{2}(C_1 + C_2)$ and C_1C_2 denote the mean curvature and the Gaussian curvature on the surface. Since the membrane is taken to be homogeneous within each domain, the bending rigidities $\kappa^{(\alpha)}$, $\kappa^{(\beta)}$, $\kappa_G^{(\alpha)}$, and $\kappa_G^{(\beta)}$ as well as the spontaneous curvatures $C_0^{(\alpha)}$ and $C_0^{(\beta)}$ are constants.

The model defined by Eqs. (2)–(6) is the spontaneous curvature model for inhomogeneous vesicles [38]. The model neglects the coupling of the two monolayers, which would be important if the flip-flop of the lipid molecules between the two monolayers was strongly suppressed. For phospholipid-cholesterol mixtures, however, this coupling should not be relevant since cholesterol molecules have a relatively high rate of flip-flop [27].

With the assumption that shape changes of the membrane do not affect the thermodynamics of the binary system, the surface areas $A^{(\alpha)}$ and $A^{(\beta)}$ are fixed by the numbers N_A and N_B of the lipid molecules. The surface densities of the free energy $f^{(\alpha)}$ and $f^{(\beta)}$ are also constant. Therefore, the bulk contribution to F_m in Eq. (3) can be omitted as a constant contribution. In order to take the constraints of fixed areas $A^{(\alpha)}$ and $A^{(\beta)}$ into account, two Lagrange multipliers $\Sigma^{(\alpha)}$ and $\Sigma^{(\beta)}$ are introduced. The shape of the vesicle is then described as the minimum of the functional

$$\begin{aligned}\hat{F} \equiv & \int_\alpha dA \left[\frac{\kappa^{(\alpha)}}{2}(C_1 + C_2 - C_0^{(\alpha)})^2 + \kappa_G^{(\alpha)} C_1 C_2\right] \\ & + \int_\beta dA \left[\frac{\kappa^{(\beta)}}{2}(C_1 + C_2 - C_0^{(\beta)})^2 + \kappa_G^{(\beta)} C_1 C_2\right] \\ & + \int_{\partial\alpha} dl\, \sigma + \Sigma^{(\alpha)} A^{(\alpha)} + \Sigma^{(\beta)} A^{(\beta)} + PV \quad ,\end{aligned} \tag{7}$$

where P is the Lagrange multiplier for the enclosed volume or, alternatively, the pressure difference between the inside and the outside of the vesicle.

B. Shape equations and matching conditions

For homogeneous vesicles, the calculation of axisymmetric shapes of minimal bending energy has been studied by several groups; see, e.g., [42,43,6]. In the following, we will derive the corresponding shape equations that determine axisymmetric stationary shapes of the functional $\hat{F}$ as given by (7). First, the axisymmetric shape is parametrized by the arclength S of the contour as shown in Fig. 1. The contour is described by the functions $R(S)$, $Z(S)$, and $\psi(S)$, where R is the distance of the

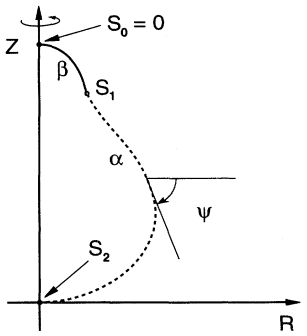

FIG. 1. Parametrization of an axisymmetric shape that consists of two domains α and β. The coordinate along the symmetry axis is denoted Z, R is the distance from this axis, ψ is the tilt angle of the contour, and S is the arclength of the contour. The domain boundary is located at $S = S_1$.

axis of rotational symmetry, Z is the coordinate along this axis, and ψ is the tilt angle of the contour. We will now focus on the case of vesicles that consist of two domains, denoted α and β. The domain β corresponds to the interval $S_0 = 0 < S < S_1$ and the domain α is described by the interval $S_1 < S < S_2$. The axisymmetric domain boundary is located at $S = S_1$.

This parametrization is convenient to describe the shape and to solve the shape equations. However, it turns out that since S_1, $R(S_1)$, and $\psi(S_1)$ cannot be varied independently, this parametrization leads to difficulties in the variational calculation if the position of the domain boundary is varied. We therefore use a generalized parametrization to carry out the variation. The result is then reparametrized by the arclength S. This method, which is described in Appendix A, leads to the shape equations (A13) and (A14) for the contour line. These shape equations reduce within each domain to the well known shape equations for vesicles of spherical topology [42,6,7]. Furthermore, as a result of the variational method, one obtains the matching conditions (A21) and (A22) for the contour at the domain boundary at $S = S_1$.

Note that the matching conditions (A21) and (A22) do not determine the shape of the domain boundary in a unique way. We will assume that the shape is smooth at the domain boundary, i.e., that the functions $R(S)$, $Z(S)$, and $\psi(S)$ are continuous at $S = S_1$. This assumption should be valid in a situation where the membrane has a continuous bilayer structure at the domain boundary. If, however, the molecular structure at the domain boundary deviates from a smooth bilayer, other matching conditions are conceivable. One could, for example, allow for a discontinuity of $\psi(S)$ at $S = S_1$ that would alter the constraints for the variations at the domain boundary and would therefore lead to modified matching conditions.

III. BUDDING INDUCED BY INTRAMEMBRANE DOMAINS

Equilibrium shapes of vesicles with two domains are studied in the framework of the model introduced in the previous section. Stationary shapes are obtained by solving the shape equations (A13) and (A14) together with the matching conditions (A21) and (A22).

One difference between homogeneous and inhomogeneous vesicles is important to note. For homogeneous vesicles with $\kappa_G^{(\alpha)} = \kappa_G^{(\beta)}$ the Gaussian curvature energy is a topological invariant that can be neglected since it does not affect the shape of a vesicle. In contrast, the Gaussian curvature is relevant for the shape of inhomogeneous vesicles if $\kappa_G^{(\alpha)} \neq \kappa_G^{(\beta)}$ [38]. However, in this section we focus on the discussion of the simplified situation $\kappa_G^{(\alpha)} = \kappa_G^{(\beta)}$, where F_G can be neglected. The effect of the Gaussian curvature energy on the shape transitions is then discussed in Sec. IV.

Two cases will be considered. (i) The water is essentially free of molecules that cannot permeate the bilayer membrane. In such a situation, the volume can adjust and there is no volume constraint on the vesicle. (ii) There are some molecules within the aqueous solution that cannot permeate the bilayer. The resulting osmotic pressure leads to a constraint on the reduced volume

$$v \equiv \frac{V}{(4\pi/3)R_0^3} \quad . \tag{8}$$

Here R_0 is the vesicle size defined by $A^{(\alpha)} + A^{(\beta)} \equiv 4\pi R_0^2$.

A. No volume constraint

For a vesicle with freely adjustable volume, the equilibrium shape is characterized by $P = 0$, i.e., there is no pressure difference across the bilayer. We first discuss the most simple case of identical bending rigidities $\kappa = \kappa^{(\alpha)} = \kappa^{(\beta)}$ of the domains and vanishing spontaneous curvatures $C_0^{(\alpha)} = C_0^{(\beta)} = 0$. The shape of the vesicle is then controlled by two dimensionless parameters: the relative domain size

$$x \equiv \frac{A^{(\beta)}}{A^{(\alpha)} + A^{(\beta)}} \tag{9}$$

and the reduced line tension

$$\lambda \equiv \sigma R_0/\kappa^{(\beta)} = R_0/\xi \quad . \tag{10}$$

Here $\xi \equiv \kappa^{(\beta)}/\sigma$ is the invagination length, which governs the competition between line tension and bending.

1. *Energy diagrams*

The energy F is displayed in Fig. 2 as a function of λ for different values of x. All curves start for $\lambda = 0$ with a sphere and energy $F/8\pi\kappa = 1$. For increasing λ, the line energy increases and the shape begins to change. This state of the vesicle is called the *incomplete bud*. For larger values of λ, the energy exhibits a Gibbs loop. Since

$$\frac{\partial F}{\partial \lambda} = \frac{2\pi\kappa}{R_0} R(S_1) \tag{11}$$

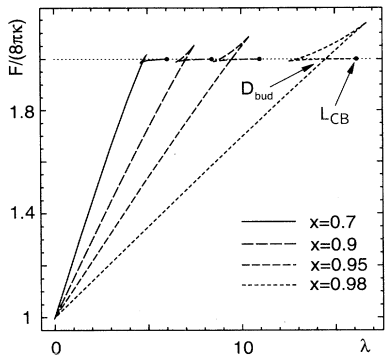

FIG. 2. Total energy F as a function of the reduced line tension λ for different values of the relative domain size x and no constraint on the volume. The energy exhibits a Gibbs loop, indicating that a discontinuous transformation $D_{\rm bud}$ between an incomplete and a complete bud occurs. The complete bud has a finite neck that closes continuously at the limit shapes $L_{\rm CB}$.

determines the radius $R(S_1)$ of the vesicle at the domain boundary, the discontinuity of $\partial F/\partial\lambda$ at the point $D_{\rm bud}$ corresponds to a shape transformation between an incomplete bud and a *complete bud*. At this shape transformation, the line energy decreases and a small neck is formed. As λ is further increased, the neck diameter $R(S_1)$ vanishes at the limit shape $L_{\rm CB}$. This limit shape consists of two spheres and has an energy $F/8\pi\kappa = 2$.

Budding also occurs for fixed λ and increasing domain size x. In Fig. 3 the energy F as a function of x together with some corresponding shapes is displayed for fixed $\lambda = 7$. A discontinuous budding transition $D_{\rm bud}$ occurs with increasing domain size. The incomplete bud becomes metastable at $D_{\rm bud}$ and unstable at $M_{\rm IB}$. At $x \simeq 0.18$, a singular limit shape $L_{\rm CB}$ with infinitesimal neck occurs.

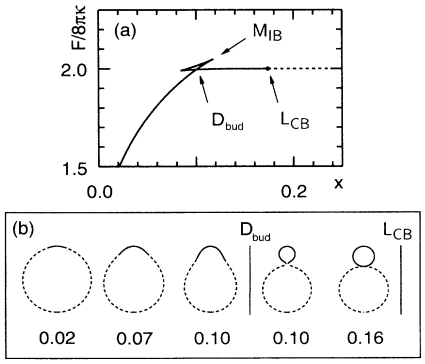

FIG. 3. (a) Total energy F as a function of the relative domain size x for fixed line tension $\lambda = 7$ and no constraint on the volume. A discontinuous budding transition $D_{\rm bud}$ occurs with increasing domain size. The incomplete bud becomes metastable at $D_{\rm bud}$ and unstable at $M_{\rm IB}$. At $L_{\rm CB}$, a singular limit shape with closed neck occurs. A sequence of corresponding shapes is displayed in (b) for different values of x.

The slope of the function $F(x)$ can be expressed by the tensions

$$\Sigma^{(\alpha)} = \left(\frac{\partial F}{\partial A^{(\alpha)}}\right)_{A^{(\beta)}}, \quad \Sigma^{(\beta)} = \left(\frac{\partial F}{\partial A^{(\beta)}}\right)_{A^{(\alpha)}} , \tag{12}$$

where the index denotes the variable that is kept constant. Now

$$\frac{\partial F}{\partial x} = A\left(\frac{\partial F}{\partial A^{(\beta)}}\right)_{A} = A(\Sigma^{(\beta)} - \Sigma^{(\alpha)}) \quad . \tag{13}$$

Here $A \equiv A^{(\alpha)} + A^{(\beta)}$ is the total area of the two domains. The tension difference $\Sigma^{(\beta)} - \Sigma^{(\alpha)}$ can be related to the geometry of the shape at the domain boundary. For two domains with $C_0^{(\alpha)} = C_0^{(\beta)}$ and $\kappa^{(\alpha)} = \kappa^{(\beta)}$, one obtains, using Eqs. (A17), (A18), and (A21),

$$\frac{\partial F}{\partial x} = -4\pi R_0^2 \cos\psi(S_1)\frac{\sigma}{R(S_1)} \quad . \tag{14}$$

The sign of $\partial F/\partial x$ is therefore determined by the tilt angle $\psi(S_1)$ of the shape at the domain boundary.

2. General neck condition

The complete buds formed by domain growth have a finite neck diameter that vanishes at the limit shape $L_{\rm CB}$. For $P = 0$, this limit shape consists of two spheres, formed by the α and the β domain, respectively. Both spheres are connected by an infinitesimal neck that contains the domain boundary.

These limit shapes $L_{\rm CB}$ satisfy a simple condition for the curvatures of the adjacent spheres at the neck. Such a neck condition has originally been introduced for homogeneous vesicles where an infinitesimal neck can only exist for $C_0 \neq 0$ [6,44]. For limit shapes of inhomogeneous vesicles, this neck condition is now generalized.

The numerical study of the limit shapes $L_{\rm CB}$ reveals that these shapes can all be described by the relation [38]

$$\kappa^{(\alpha)}M^{(\alpha)} + \kappa^{(\beta)}M^{(\beta)} = \frac{1}{2}(\kappa^{(\alpha)}C_0^{(\alpha)} + \kappa^{(\beta)}C_0^{(\beta)} + \sigma) \quad . \tag{15}$$

Here $M^{(\alpha)}$ and $M^{(\beta)}$ denote the mean curvatures of the domains at the point of contact. This neck condition can also be obtained by extending a simple toy model introduced by Fourcade *et al.* [44] to inhomogeneous vesicles as described in Appendix B.

The limit shapes for $P = 0$ consist of two spheres. Since $A^{(\beta)} = 4\pi R_0^2 x$ and $A^{(\alpha)} = 4\pi R_0^2(1-x)$, one has $M^{(\beta)} = 1/(R_0 x^{1/2})$ and $M^{(\alpha)} = 1/[R_0(1-x)^{1/2}]$. If these expressions are inserted into the neck condition (15), one obtains

$$\lambda_L(x) = \frac{\kappa^{(\alpha)}}{\kappa^{(\beta)}}\frac{2}{\sqrt{1-x}} + \frac{2}{\sqrt{x}} - \frac{\kappa^{(\alpha)}}{\kappa^{(\beta)}}c_0^{(\alpha)} - c_0^{(\beta)} \tag{16}$$

for the lines $\lambda = \lambda_L(x)$ of the limit shapes $L_{\rm CB}$ within the (x,λ) plane. Here $c_0^{(i)} = C_0^{(i)}R_0$ with $i = \alpha,\beta$ de-

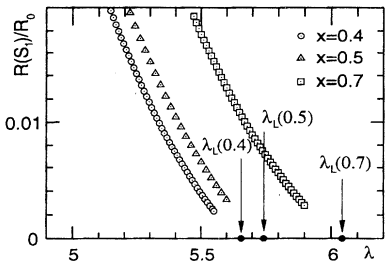

FIG. 4. Neck diameter $R(S_1)$ as a function of the line tension λ close to the limit shapes $L_{\rm CB}$ for different values of the relative domain size x and no volume constraint. The generalized neck condition (15) determines the value $\lambda = \lambda_L(x)$ where the stationary shapes become singular with $R(S_1) = 0$. The plot shows that the neck condition (15) agrees with the numerical solutions of the shape equations.

noting the dimensionless spontaneous curvatures of the domains. For the simple case of domains without spontaneous curvatures and $\kappa^{(\alpha)} = \kappa^{(\beta)}$, Eq. (16) reduces to

$$\lambda_L(x) = \frac{2}{\sqrt{x}} + \frac{2}{\sqrt{1-x}} \quad . \tag{17}$$

The neck condition (15) has been checked by extrapolating the neck diameter $R(S_1)$ as a function of λ close to the limit shape $L_{\rm CB}$. As an example, the scaled neck diameter $R(S_1)/R_0$ of stationary shapes is shown in Fig. 4 as a function of λ for different values of x. The lines end up for $R(S_1)/R_0 \simeq 0.02$ where the numerical determination of stationary shapes breaks down. The extrapolation of these curves to $R(S_1) = 0$ leads to a value for $\lambda_L(x)$ that is in perfect agreement with Eq. (17).

For a homogeneous membrane, with $C_0^{(\alpha)} = C_0^{(\beta)} \equiv C_0$, $\kappa^{(\alpha)} = \kappa^{(\beta)}$, and $\sigma = 0$, Eq. (15) reduces to the well known neck condition $M^{(\alpha)} + M^{(\beta)} = C_0$ for homogeneous vesicles. For two identical domains and zero spontaneous curvatures, the neck condition

$$M^{(\alpha)} + M^{(\beta)} = \sigma/2\kappa \tag{18}$$

determines the line tension σ, which is necessary in order to stabilize an infinitesimal neck against the tendency of the bending energy to open it.

3. Phase diagram

The phase diagram for domain induced budding is shown in Fig. 5(a) as a function of relative domain size x and line tension λ for two identical domains with bending rigidities $\kappa^{(\alpha)} = \kappa^{(\beta)}$ and spontaneous curvatures $C_0^{(\alpha)} = C_0^{(\beta)} = 0$. This phase diagram has been obtained from several energy diagrams as shown in Figs. 2 and 3. Since both domains have identical elastic properties, the phase diagram is symmetric under the transformation $x \to -1 + x$, which corresponds to an exchange of both domains. The line $\lambda_L(x)$ of limit shapes $L_{\rm CB}$ is given by (17). For $\lambda > \lambda_L(x)$, the same limit shapes are still shapes of lowest energy. However, they are no longer stationary shapes but represent boundary minima.

Along the line $D_{\rm bud}$ with $\lambda = \lambda_D(x)$, discontinuous shape transitions between an incomplete bud and a complete bud occur. For this line, no analytic expression is known. In order to study the effect of different values of the bending rigidities $\kappa^{(i)}$ and the spontaneous curvatures $C_0^{(i)}$ on the phase diagram, it is very helpful to discuss an approximation for this line, which will be denoted by $\lambda = \tilde{\lambda}_D(x)$. The discontinuous transition occurs when the energies of the incomplete bud and of the complete bud are the same. The incomplete bud can be approximated by a sphere with a spherical cap and the complete bud by two spheres. This approximation leads to a budding transition at $\lambda = \tilde{\lambda}_D(x)$ with

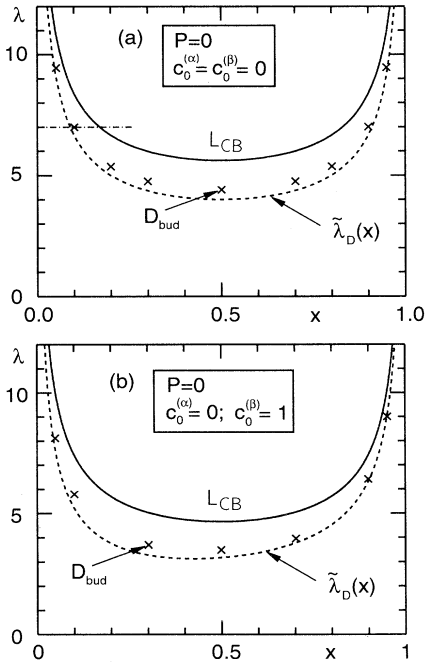

FIG. 5. (a) Phase diagram as a function of the line tension λ and domain size x for vanishing spontaneous curvatures $c_0^{(\alpha)} = c_0^{(\beta)}$ and no volume constraint, i.e., pressure $P = 0$. At the point $D_{\rm bud}$, a discontinuous transition between an incomplete bud and a complete bud occurs. The neck of the complete bud closes at the limit shape $L_{\rm CB}$, where the shape becomes completely vesiculated. This line is described by the function $\lambda_L(x)$ as given by (17). The dashed line $\tilde{\lambda}_D(x)$ is the approximation for the transition line $D_{\rm bud}$ as given by (19). The dotted-dashed line for $\lambda = 7$ corrresponds to the sequence of shapes shown in Fig. 3. (b) Same diagram but for $c_0^{(\alpha)} = 0$ and $c_0^{(\beta)} = 1$.

$$\tilde{\lambda}_D(x) \equiv \frac{2}{\kappa^{(\beta)}\sqrt{x-x^2}}\Big\{\kappa^{(\alpha)}x+\kappa^{(\beta)}(1-x) +\kappa^{(\alpha)}c_0^{(\alpha)}[1-x-(1-x)^{1/2}] +\kappa^{(\beta)}c_0^{(\beta)}(x-x^{1/2})\Big\}. \quad (19)$$

For domains with identical bending rigidities and without spontaneous curvatures, this expression simplifies and reads

$$\tilde{\lambda}_D(x) = \frac{2}{\sqrt{x-x^2}} \quad . \quad (20)$$

The approximation $\tilde{\lambda}_D$ underestimates the value of λ where budding occurs, i.e., $\tilde{\lambda}_D(x) \lesssim \lambda_D(x)$.

As a second example, the phase diagram for $\kappa^{(\alpha)} = \kappa^{(\beta)}$, $c_0^{(\alpha)} = 0$, and $c_0^{(\beta)} = 1$ is shown in Fig. 5(b). In this case the line $L_{\rm CB}$ is still symmetric with respect to $x \to -x+1$. The discontinuous phase boundary $D_{\rm bud}$, on the other hand, is asymmetric. The approximation $\tilde{\lambda}_D$ qualitatively describes the shape of this transformation line.

The symmetry between the two domains is also broken if the bending rigidities $\kappa^{(\alpha)}$ and $\kappa^{(\beta)}$ are different. In this case, the line $L_{\rm CB}$ is not symmetric with respect to $x \to 1-x$, according to Eq. (16). If the bending rigidity $\kappa^{(\beta)}$ of the growing domain is larger than $\kappa^{(\alpha)}$, budding will occur for smaller values of x and λ and a smaller bud will be formed. The locus of the corresponding transition is also well approximated by $\tilde{\lambda}_D(x)$ as given by Eq. (19).

B. Fixed volume

1. *Equilibrium shapes for fixed reduced volume*

Domain growth provides a local mechanism for budding. Therefore, one expects that any global constraint will act to suppress it. This is indeed what is found for the constraint of fixed volume. This effect is most pronounced for $v \simeq 1$, where the shape cannot deviate from a sphere and therefore only very small buds are possible.

Now consider vesicles of the same reduced volume $v < 1$ with different relative domain sizes x. For $x = 0$, the membrane is homogeneous. It is well known that in the case of homogeneous vesicles with vanishing spontaneous curvature the shape of minimal energy is a prolate within the interval $0.65 \lesssim v < 1$ of the reduced volume [6]. If x is now increased to a finite value, a small domain β exists, which will be located on one of the two "caps" of the prolate since this configuration is most symmetric and energetically favored. In the following, we restrict our discussion to the case of prolates and look at values of the reduced volume that are sufficiently large so that prolates are the shapes of minimal energy.

The energy F as a function of x for $\lambda = 12$ and $v = 0.8$ is shown in Fig. 6 together with some corresponding shapes. Again, the formation of a complete bud with a finite neck diameter occurs at $D_{\rm bud}$. The neck size

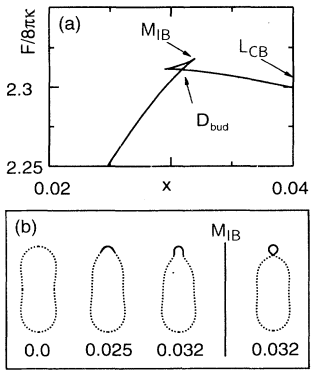

FIG. 6. (a) Energy F as a function of the relative domain size x for fixed $v = 0.8$ and $\lambda = 12$. A discontinuous transition occurs at $D_{\rm bud}$. For growing domain size, the incomplete bud becomes metastable at $D_{\rm bud}$ and unstable at $M_{\rm IB}$. The limit shape $L_{\rm CB}$ occurs for $x \simeq 0.56$. A corresponding sequence of shapes is shown in (b) for different values of x.

vanishes for $x \simeq 0.56$ at a limit shape $L_{\rm CB}$. The slope $\partial F/\partial x$ is again described by Eq. (14).

The complete phase diagram for $v = 0.8$ is displayed in Fig. 7. It reveals that the line $D_{\rm bud}$ ends up in a critical point at $(x,\lambda) = (x_c,\lambda_c) \simeq (0.05, 9.8)$. For $\lambda_c > \lambda > \lambda_{\rm sp} \simeq 6.9$, budding occurs continuously when a limit shape at $L_{\rm CB}$ is reached. This limit shape consists of a spherical bud with area $A^{(\beta)} = 4\pi R_0^2 x$ and volume $V^{(\beta)} = (4\pi/3)R_0^3 x^{3/2}$, which is attached to a prolate, characterized by its reduced volume

$$\tilde{v}_P \equiv \frac{V-V^{(\beta)}}{(4\pi/3)(A^{(\alpha)}/4\pi)^{3/2}} = \frac{v-x^{3/2}}{(1-x)^{3/2}} \quad . \quad (21)$$

Both parts are connected by an infinitesimal neck. Along the line $L_{\rm CB}$, the prolate volume $\tilde{v}_P$ increases with in-

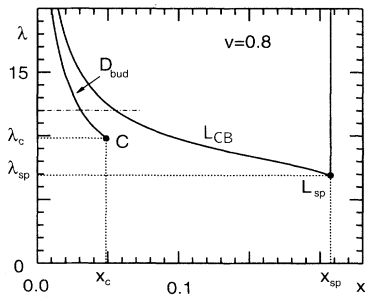

FIG. 7. Phase diagram as a function of λ and x for reduced volume $v = 0.8$. The line $D_{\rm bud}$ of discontinuous budding transitions ends in a critical point C with $(x,\lambda) = (x_c,\lambda_c)$. For $\lambda_c > \lambda > \lambda_{\rm sp}$, budding occurs continuously for increasing x when the limit shape $L_{\rm CB}$ is reached. The line of limit shapes ends in the point $L_{\rm sp}$ which corresponds to a limit shape consisting of two spheres. The dotted-dashed line for $\lambda = 12$ corresponds to the energy diagram as shown in Fig. 6.

creasing x. The line ends at $(x,\lambda) = (x_{\rm sp},\lambda_{\rm sp}) \simeq (0.21, 6.9)$, where the prolate becomes a sphere with $\tilde{v}_P = 1$, which implies the relation

$$1 = \frac{v - x_{\rm sp}^{3/2}}{(1-x_{\rm sp})^{3/2}} \tag{22}$$

at the point $L_{\rm sp}$.

Extrapolation of the neck radius of numerically determined shapes as a function of λ shows that the shapes $L_{\rm CB}$ are again described by the general neck condition (15) introduced in Sec. III A above. This neck condition determines the position $[x, \lambda_L(x,v)]$ of the limit shapes $L_{\rm CB}$ in the (x,λ) plane. The phase boundary $L_{\rm CB}$ can therefore be obtained by using Eq. (15) as described in Appendix C.

2. *Budding induced by osmotic deflation*

Shape transformations can also be induced by changing the reduced volume osmotically. In this type of experiment, a sequence of equilibrium shapes is generated that differ in their reduced volume.

Starting, for example, with a vesicle close to a sphere and $v \simeq 1$, a decrease of the reduced volume v leads to budding if the line tension is sufficiently large as will be shown now. For decreasing v, the line energy can be lowered by forming a bud. An example for such a situation is shown in Fig. 8(a). In this figure the energy is plotted for reduced line tension $\lambda = 9$ and relative domain size $x = 0.1$ as a function of v. The diagram reveals that for decreasing reduced volume the energy strongly decreases until it reaches the limit shape $L_{\rm sp}$, where two spheres are connected by an infinitesimal neck.

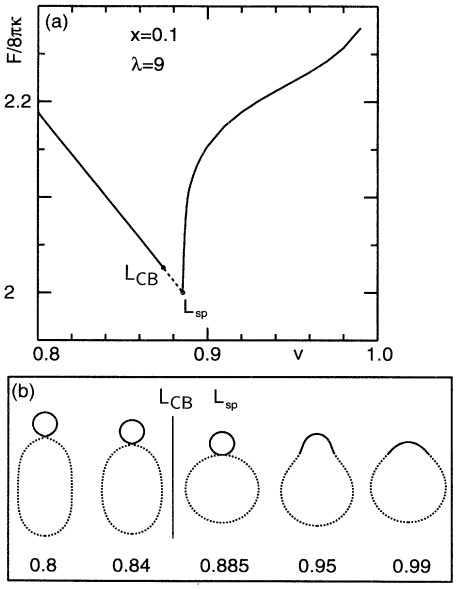

FIG. 8. (a) Energy F as a function of the reduced volume v for line tension $\lambda = 9$ and relative domain size $x = 0.1$. The limit shape $L_{\rm CB}$ consists of a prolate and a sphere, while the shape $L_{\rm sp}$ consists of two spheres. The broken line connecting both stationary limit shapes gives the energy of boundary minima with vanishing neck diameter. A corresponding sequence of shapes is shown in (b) for different values of v.

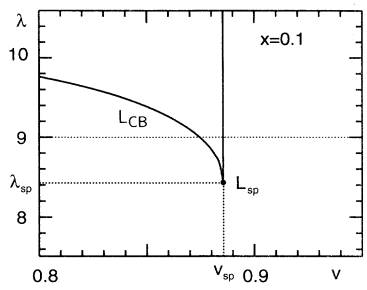

FIG. 9. Phase diagram as a function of the line tension λ and reduced volume v for fixed relative domain size $x = 0.1$. For decreasing v, budding occurs continuously at $L_{\rm sp}$, which is a stationary limit shape consisting of two spheres. At $L_{\rm CB}$, the neck opens again. Budding does not occur for $\lambda < \lambda_{\rm sp}$. The dotted line for $\lambda = 9$ corresponds to the sequence of shapes as shown in Fig. 8(b).

A further decrease of v leads to a sequence of boundary minima with infinitesimal neck until the shape $L_{\rm CB}$ is reached and the neck opens again. However, the neck diameter stays relatively small up to $v = 0.8$; see Fig. 8(b). The phase diagram as a function of λ and v is shown in Fig. 9. For decreasing v only two situations occur. For $\lambda > \lambda_{\rm sp} \simeq 8.43$, the vesicle forms the limit shape $L_{\rm sp}$ consisting of two spheres as soon as one reaches the reduced volume $v = v_{\rm sp}$. Since the volumes of the two spheres are given by $V^{(\alpha)} = (4\pi/3)R_0^3(1-x)^{3/2}$ and $V^{(\beta)} = (4\pi/3)R_0^3 x^{3/2}$, respectively, one has the relation

$$v_{\rm sp} = (1-x)^{3/2} + x^{3/2} \quad . \tag{23}$$

For $\lambda < \lambda_{\rm sp}$, the shape changes without the formation of a bud. If the relation (23) is inverted, one obtains $x = x(v_{\rm sp})$, which determines $\lambda_{\rm sp} = \lambda_L(x(v_{\rm sp}), v_{\rm sp})$. The line $L_{\rm CB}$ can be obtained from the neck condition (15) as described in Appendix C.

IV. ROLE OF THE GAUSSIAN CURVATURE

A. Gaussian curvature energy of axisymmetric shapes

The vesicle shapes studied so far have been obtained from the bending energy F_b without taking the Gaussian curvature energy F_G into account. For homogeneous vesicles, this energy is a topological invariant due to the Gauss–Bonnet theorem. The Gaussian curvature energy (6) of an inhomogeneous vesicle with homogeneous domains can be simplified by the Gauss–Bonnet

theorem, which leads to [45]

$$F_G = -(\kappa_G^{(\alpha)} - \kappa_G^{(\beta)}) \oint_{\partial\alpha} dl\, C_g + 2\pi(\kappa_G^{(\alpha)} + \kappa_G^{(\beta)}) \quad . \tag{24}$$

Here dl is the line element along the domain boundary and C_g is the geodesic curvature along this line. The orientation of the line element has been chosen in such a way that one moves around the β domain in a clockwise fashion when one looks down onto this domain from a position outside of the vesicle. The geodesic curvature can be expressed as [45]

$$C_g \equiv \left(\mathbf{n} \times \frac{d\mathbf{R}}{dl}\right) \cdot \frac{d^2\mathbf{R}}{dl^2} \quad , \tag{25}$$

where $\mathbf{R}(l)$ is a parametrization of the domain boundary with $|d\mathbf{R}/dl| = 1$ and $\mathbf{n}(l)$ denotes the normals of the surface along the domain boundary. Note that the value of the geodesic curvature C_g changes its sign if the orientation of the line element is reversed and one moves along the domain boundary in the opposite direction.

The first term in Eq. (24) depends on the shape of the vesicle while the second contribution is a constant that will be omitted in the following. For an axisymmetric shape parametrized by its contour line, Eq. (24) can be simplified further. The domain boundary at $S = S_1$ can be written as

$$\mathbf{R}(l) \equiv \begin{pmatrix} R(S_1)\sin\phi(l) \\ R(S_1)\cos\phi(l) \\ Z(S_1) \end{pmatrix} \quad , \tag{26}$$

where $\phi(l) \equiv l/R(S_1)$. Using

$$\mathbf{n}(l) \equiv \begin{pmatrix} \sin\psi(S_1)\sin\phi(l) \\ \sin\psi(S_1)\cos\phi(l) \\ \cos\psi(S_1) \end{pmatrix} \quad , \tag{27}$$

the geodesic curvature simply reads

$$C_g(l) = -\cos\psi(S_1)/R(S_1) \quad . \tag{28}$$

Inserting this expression into Eq. (24), one obtains [38]

$$F_G = 2\pi(\kappa_G^{(\alpha)} - \kappa_G^{(\beta)})\cos\psi(S_1) \quad , \tag{29}$$

where the constant term has been omitted. This contribution has been included in the derivation of the shape equations and the matching conditions as described in Appendix A.

B. Energy diagrams

The numerical solutions of the shape equations (A13) and (A14) together with the matching conditions (A21) and (A22) show that the structure of the energy diagrams changes significantly if the Gaussian curvature energy term with $\kappa_G^{(\alpha)} \neq \kappa_G^{(\beta)}$ is taken into account. The total energy F is shown in Fig. 10(a) as a function of x for $(\kappa_G^{(\alpha)} - \kappa_G^{(\beta)})/\kappa = -1$ and $\lambda = 7$ for $\kappa = \kappa^{(\alpha)} = \kappa^{(\beta)}$ and

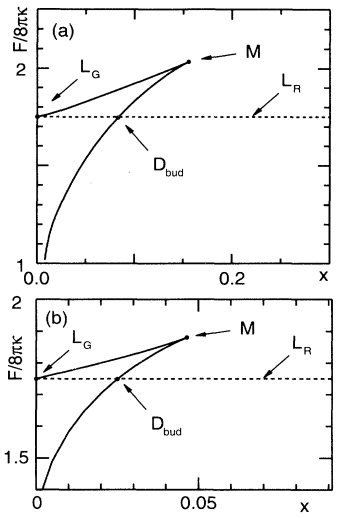

FIG. 10. (a) Energy F as a function of the relative domain size x for line tension $\lambda = 7$ and pressure $P = 0$ for two domains of different Gaussian bending rigidity $(\kappa_G^{(\alpha)} - \kappa_G^{(\beta)})/\kappa = -1$. The same diagram but with $(\kappa_G^{(\alpha)} - \kappa_G^{(\beta)})/\kappa = 1$ is displayed in (b). At $D_{\rm bud}$, a discontinuous transition between an incomplete bud and a vesiculated configuration L_R occurs. The branch of stationary shapes ends up at the limit shape L_G.

$P = 0$. The same situation but with $(\kappa_G^{(\alpha)} - \kappa_G^{(\beta)})/\kappa = 1$ is displayed in Fig. 10(b). The branches of stationary shapes end up in a limit shape L_G at $x = 0$. The broken lines with $F/(8\pi\kappa) = 1.75$ describe boundary minima L_R, which for large values of x are absolute minima of the energy. The shapes L_R and L_G consist of two spheres with a ratio of radii $x^{1/2}/(1-x)^{1/2}$ that are connected by an infinitesimal neck.

At the point where the branch of stationary shapes meets the line L_R, a discontinuous transition between an incomplete bud and a complete bud occurs. In contrast to the case without a Gaussian curvature term, the complete bud corresponding to the shapes L_R is a limit shape that has an infinitesimal neck already at the transition. At the limit of metastability M, the stationary shapes become unstable and a bud must be formed for increasing x.

These plots can be compared with the diagram shown in Fig. 2 for the corresponding case with $\kappa_G^{(\alpha)} = \kappa_G^{(\beta)}$. In this case, a finite neck is formed at the discontinuous transition. This neck closes continuously at a stationary limit shape $L_{\rm CB}$. For $(\kappa_G^{(\alpha)} - \kappa_G^{(\beta)})/\kappa = \pm 1$, small but finite necks correspond to the unstable part of the branch of stationary shapes. The Gibbs loop and the energy barrier are much larger compared to the case where $\kappa_G^{(\alpha)} = \kappa_G^{(\beta)}$.

The two diagrams shown in Fig. 10 reveal the difference between the situations with $\kappa_G^{(\alpha)} > \kappa_G^{(\beta)}$ and with $\kappa_G^{(\alpha)} < \kappa_G^{(\beta)}$. While the energy diagrams look qualitatively similar in both cases, the scale of the x axis is different. For $\kappa_G^{(\alpha)} > \kappa_G^{(\beta)}$, the shape transition $D_{\rm bud}$ occurs

for smaller values of x compared to the case $\kappa_G^{(\alpha)} < \kappa_G^{(\beta)}$. This can be understood by a simple argument. For $\kappa_G^{(\alpha)} > \kappa_G^{(\beta)}$, the Gaussian bending energy F_G of a flat membrame with $\psi(S_1) = 0$ is maximal according to the relation (29). It follows from the same relation that budding leads to a decrease of F_G that attains its minimal value for $\psi(S_1) = \pi$. Therefore, the Gaussian bending energy assists the formation of a bud and the shape transition occurs for relatively small values of x. Similarly, for $\kappa_G^{(\alpha)} < \kappa_G^{(\beta)}$ the flat configuration is optimal with respect to F_G. Therefore, in the latter case, the Gaussian bending energy hinders the formation of a bud.

C. Structure of small necks

The discussion of the energy diagrams in the previous subsection indicated that the Gaussian bending energy influences the structure and the stability of small necks. For a homogeneous vesicle, an infinitesimal neck leads to a finite contribution, $\simeq -4\pi\kappa_G$, to the Gaussian bending energy. On the other hand, the normal bending energy F_b of a neck with vanishing diameter is zero.

For a vesicle consisting of two domains with different $\kappa_G^{(i)}$, the energy F_G is minimal if the neck is formed completely by the domain with small κ_G. Thus the Gaussian bending energy acts to shift the domain boundary away from the neck. For $\kappa_G^{(\alpha)} = \kappa_G^{(\beta)}$, on the other hand, the domain boundary prefers to sit in the neck at its smallest diameter.

The interaction between the neck and the domain boundary for $\kappa_G^{(\alpha)} \neq \kappa_G^{(\beta)}$ can be discussed in the limit of vanishing neck diameter. The limit shapes L_G and the boundary minima L_R consist of two spheres connected by an infinitesimal neck. For vanishing neck diameter, the bending energy F_b of the neck and the line energy F_l vanish. The total energy of these shapes is then given by

$$F = 8\pi(\kappa^{(\alpha)} + \kappa^{(\beta)}) + 2\pi(\kappa_G^{(\alpha)} - \kappa_G^{(\beta)})\cos\psi(S_1) \quad . \quad (30)$$

The first term in Eq. (30) represents the bending energy of the two spheres α and β for $c_0^{(\alpha)} = c_0^{(\beta)} = 0$ and the second term is the contribution of F_G that depends on the shape.

As shown schematically in Fig. 11, the angle $\psi(S_1)$ can be chosen in the interval $0 < \psi < \pi$ without affecting the limit shape. Thus, for $\kappa_G^{(\alpha)} > \kappa_G^{(\beta)}$ and $\kappa_G^{(\alpha)} < \kappa_G^{(\beta)}$, there exist two different minima with $\psi(S_1) = \pi$ and $\psi(S_1) = 0$. In both cases, the domain with smaller $\kappa_G^{(i)}$ forms the neck. On the other hand, the limit shapes $L_{\rm CB}$ for $\kappa_G^{(\alpha)} = \kappa_G^{(\beta)}$ are described by $\psi(S_1) = \pi/2$.

It is interesting to understand if the limit shapes L_G can also be characterized by a neck condition. A neck condition fixes the position of stationary limit shapes in the (x, λ) plane. The analysis of the limit shapes L_G reveals that they always exist either for $x = 0$ or for $\lambda = 0$. The position of the shapes L_G in the (x, λ) plane therefore does not depend on the local curvatures of the surface and the general neck condition as given by Eq. (15) does not apply to these limit shapes.

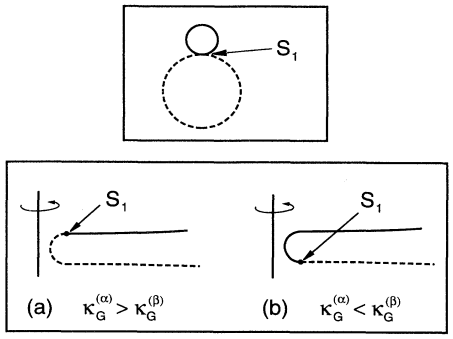

FIG. 11. Schematic representation of the neck region of the boundary minima L_R and the stationary limit shapes L_G. For vanishing neck diameter $R(S_1) \simeq 0$ one finds (a) $\psi(S_1) = \pi$ for $\kappa_G^{(\alpha)} > \kappa_G^{(\beta)}$ and (b) $\psi(S_1) = 0$ for $\kappa_G^{(\alpha)} < \kappa_G^{(\beta)}$.

D. Phase diagrams

The structure of the energy diagrams for $\kappa_G^{(\alpha)} \neq \kappa_G^{(\beta)}$ and $P = 0$ leads to phase diagrams with a transition line $D_{\rm bud}$, which is similar to the line $D_{\rm bud}$ in the phase diagram for $\kappa_G^{(\alpha)} = \kappa_G^{(\beta)}$ as shown in Fig. 5. However, for $\kappa_G^{(\alpha)} \neq \kappa_G^{(\beta)}$, the phase diagram lacks a line $L_{\rm CB}$, since a continuous closure of a small neck at a stationary limit shape does not occur in this case.

More interesting is the case of fixed reduced volume v. For $\kappa_G^{(\alpha)} = \kappa_G^{(\beta)}$ and $v = 0.8$, the line $D_{\rm bud}$ ends up in a critical point. Since for $\kappa_G^{(\alpha)} \neq \kappa_G^{(\beta)}$ the energy diagrams always end up with a limit shape L_G at $x = 0$ and $\lambda = 0$, the Gibbs loop cannot close and thus a critical point cannot exist. In Fig. 12 the corresponding phase diagram for $(\kappa_G^{(\alpha)} - \kappa_G^{(\beta)})/\kappa = -1$ and $v = 0.8$

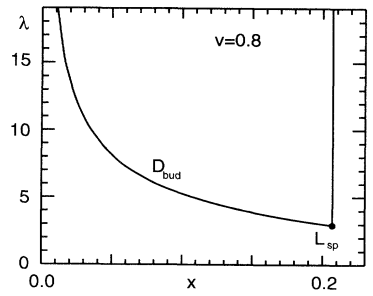

FIG. 12. Phase diagram as a function of line tension λ and domain size x for reduced volume $v = 0.8$ and Gaussian curvature modulus $(\kappa_G^{(\alpha)} - \kappa_G^{(\beta)})/\kappa = -1$. Budding occurs discontinuously at the line $D_{\rm bud}$. This line ends in the point $L_{\rm sp}$.

is shown for $\kappa^{(\alpha)} = \kappa^{(\beta)}$ and $c_0^{(\alpha)} = c_0^{(\beta)} = 0$. Along the line $D_{\rm bud}$, discontinuous budding transitions between an incomplete bud and a complete bud with closed neck occur. Above the line $D_{\rm bud}$, shapes of minimal energy are boundary minima L_R consisting of a prolate α and a sphere β. Both shapes are connected by an infinitesimal neck. The reduced volume $\tilde{v}_P$ of the prolate is given by Eq. (21). These limit shapes exist for $x < x_{\rm sp}$, defined in Eq. (22). For $x > x_{\rm sp}$, budding is suppressed by the volume constraint.

V. GROWTH OF NUCLEATED DOMAINS

In general, a multicomponent membrane will exhibit a two-phase coexistence region as a function of temperature and composition. This two-phase region exhibits (i) a nucleation regime, in which one has to overcome an energy barrier in order to form a "critical" domain, and (ii) a regime of spinodal decomposition, in which such a barrier is absent.

Now consider a membrane that is initially prepared in a homogeneous state within the one-phase region and is then quenched into the two-phase region. Let us first assume that the membrane is quenched deep into the spinodal decomposition regime. If the phase separation process is sufficiently fast, it may lead to complete phase separation within the membrane and will thus create vesicles consisting of one α and one β domain. The equilibrium shape of these vesicles, which has been described in Secs. II and III above, will often exhibit a bud containing the smaller domain.

Now let us assume that the membrane is quenched into the nucleation regime. If the activation energy for the critical domain is sufficiently large, only one domain will be nucleated initially and one may study the growth of such a domain. Since the growth of this domain is limited by diffusion, the growth may proceed rather slowly [34,35]. One may then use an adiabatic approximation in which the shape is taken to adjust to the domain size at any given time.

Since the volume will stay constant during this process, one will then consider a trajectory in the phase diagram for fixed volume. Since the growing domain leads to an increase in the relative domain size x, the trajectory of such a process is given by a straight line parallel to the x axis. An example for such a trajectory is shown as a dashed line for $\lambda = 12$ in Fig. 7. This trajectory corresponds to the sequence of shapes as shown in Fig. 6(b). In this figure the incomplete bud is displayed up to the point $M_{\rm IB}$, where it becomes unstable. At this point, the vesicle therefore has to undergo a budding process. Simple estimates indicate that the lateral tension that builds up during this process is sufficient to rupture the membrane along the domain boundary and thus to detach the bud from the mother vesicle [34,35].

VI. DISCUSSION

In the previous sections, the shapes and shape transformations of vesicles that consist of two fluid domains that are separated by a domain boundary have been studied systematically. This study confirms and extends the results of simpler models [34,35] and shows that vesicles that contain intramembrane domains tend to form buds. Budding represents the shape transformation from the incomplete bud to the complete bud. This shape transformation can be either continuous or discontinuous. The complete bud is connected to the original vesicle by a neck with small or vanishing diameter. The structure and the stability of the small necks that occur as a result of the budding transition are strongly influenced by Gaussian bending energies. As soon as the Gaussian bending rigidities of the two domains differ, the domain boundary is pushed out of the neck and necks of finite diameter tend to become unstable and close completely.

Shape transformations of multicomponent vesicles have also been studied experimentally. In these experiments, multicomponent vesicles consisting of a mixture of sphingomyelin molecules with different chain length and vesicles consisting of phospholipid-cholesterol mixtures were used [13].

Calorimetric measurements revealed that a phase transition occurs at 41 °C in the sphingomyelin mixture. However, the structure of the coexisting phases is not known. Facets of the vesicle observed in the low-temperature phase indicate a fluid-gel coexistence. At the phase transition, small buds are forming, which immediately detach from the original vesicle (fission). The physical mechanism that leads to budding in this case remains unclear. In a second set of experiments, vesicles, consisting of a phospholipid-cholesterol mixture, were osmotically deflated. As a result, budding and fission occurred. The mechanism that drives the shape changes in this situation is again not clear. The shape transformation could be partly due to phase separation within the mixture. However, in this experiment another effect could also be important for the observed shape change: As the vesicle is osmotically deflated, water flows across the bilayer outwards. This water flow can drag some lipid molecules from the inner to the outer monolayer. An increased number of lipid molecules in the outer monolayer could lead to a tendency of the bilayer to bend and to form a bud [46]. In this experiment, budding induced by a redistribution of lipids across the bilayer cannot be distinguished from budding induced by intramembrane domains.

In order to confirm the mechanism of budding induced by intramembrane domains as studied in this paper, further experiments are necessary. A very important system for this study is the phospholipid-cholesterol mixture that exhibits a coexistence region of a cholesterol rich and a cholesterol poor phase that are both fluid [19,24–26]. The experimental data within the coexistence region are usually interpreted in terms of lateral phase separation. In principle, one could also envisage transverse phase separation for which both monolayers differ in their cholesterol concentration. However, in both situations, the coexistence region will contain a nucleation regime in which the phase separation starts with the formation of intramembrane domains.

If phospholipid-cholesterol vesicles are formed by a bi-

layer with a composition corresponding to a homogeneous phase in the phase diagram of the phospholipid-cholesterol mixture, a temperature change can move the system to the region of two-phase coexistence. In the nucleation regime of this coexistence region, small domains will grow after their nucleation. Budding will then occur when the domain size becomes comparable to the invagination length $\xi = \kappa/\sigma$. For a phospholipid-cholesterol bilayer, the bending rigidity $\kappa \simeq 4\times10^{-19}$ J, as measured by optical microscopy [47]. An estimate for the line tension can be obtained from relaxation measurements of domains in monolayers, which suggest $\sigma \simeq 10^{-12}$ J/m [21]. Thus this estimate leads to $\xi \simeq 400$ nm.

In general, the buds that will be formed as a result of domain growth in the nucleation regime are expected to be too small to be visible under the microscope. As soon as budding occurs, the original vesicle will lose area. If many buds are formed, this area loss can be detected even if the buds themselves are invisible. In order to show that the missing area is in fact hidden in small buds, additional methods are necessary. For example, the sudden occurrence of many small vesicles with a size of the order of 100 nm could be detected by light scattering.

Another way to induce budding and to generate large buds is to start with a vesicle in the homogeneous phase of the lipid mixture with a shape close to a sphere, i.e., $v \simeq 1$. Now the vesicle is moved to the coexistence region of the phase diagram. On the sphere phase separation will occur, but the shape cannot change since the constraint on the reduced volume does not allow a shape change. Two domains will form on the sphere, their relative size again depends on the composition of the original vesicle. A shape change can now be induced by osmotically deflating the vesicle, which leads to a decrease of the reduced volume. The line energy of the domain boundary can now be lowered by forming a bud. In this case, the bud formed will always consist of two spheres connected by an infinitesimal neck. A further decrease of the reduced volume can open the neck again in some cases; see Fig. 9.

The mechanism for budding induced by intramembrane domains as studied in this paper might also be important for shape changes within biological membranes [34,35]. In fact, biological membranes are lipid mixtures consisting of a large number of different molecules. Many biological membranes also contain a high fraction of cholesterol.

Budding of biological membranes is very common [18]. The small vesicles, formed as a result of budding, enclose molecules that have to be transported to a different place within the cell. The bud detaches from the original membrane and can then move away from it. Such transport vesicles could be the result of domains that form in the membrane. The existence of domains within biological membranes is now well established [48]. These domains either have a different lipid or cholesterol composition than the environment or are formed by a cluster of membrane proteins.

Cholesterol plays an important role in biological membranes [27]. A membrane with high cholesterol composition is less permeable for small molecules than a membrane with a small amount of cholesterol. Therefore, the cholesterol composition of the outer plasma membrane is relatively large, but the cholesterol concentration inside the cell is smaller [28]. In order to build up this concentration gradient of cholesterol, the cell needs a transport mechanism for cholesterol. One possible transport mechanism would be the use of transport vesicles that have a higher concentration of cholesterol compared to the membrane from which they originated by budding. This would imply that these vesicles were formed from a cholesterol-rich domain within the membrane. Domain-induced budding provides a simple mechanism for this to occur.

APPENDIX A: SHAPE EQUATIONS FOR TWO-COMPONENT VESICLES

The shape equations for a vesicle consisting of two domains α and β are derived as stationary shapes of the functional $\hat{F}$ defined in Eq. (7). The contour is parametrized by the functions $R(t)$, $Z(t)$, $\psi(t)$, and $S(t)$ of a generalized parameter t with $S(t_0) = 0$, $S(t_1) = S_1$, and $S(t_2) = S_2$. In this parametrization,

$$\hat{F} \equiv 2\pi\left[\int_0^{t_1} dt\, \mathcal{K}^{(\beta)} + \int_{t_1}^{t_2} dt\, \mathcal{K}^{(\alpha)} + \sigma R(t_1) + (\kappa_G^{(\alpha)} - \kappa_G^{(\beta)})\cos\psi(t_1)\right], \tag{A1}$$

where Eq. (29) has been used. Here

$$\mathcal{K}^{(i)} \equiv \frac{\kappa^{(i)}}{2} RS'\left(\frac{\psi'}{S'} + \frac{\sin\psi}{R} - C_0^{(i)}\right)^2 + \Sigma^{(i)} RS' + \frac{1}{2}PR^2S'\sin\psi + \gamma(R' - S'\cos\psi), \tag{A2}$$

with $i = \alpha$ or β. The primes denote derivatives with respect to t and the Lagrange multiplier function $\gamma(t)$ is introduced in order to incorporate the geometrical constraint $R' = S'\cos\psi$.

Under a variation

$$\psi(t) = \psi_0(t) + \delta\psi(t), \tag{A3}$$
$$R(t) = R_0(t) + \delta R(t), \tag{A4}$$
$$\gamma(t) = \gamma_0(t) + \delta\gamma(t), \tag{A5}$$
$$S(t) = S_0(t) + \delta S(t) \tag{A6}$$

of the shape, the functional $\hat{F}$ is varied according to

$$\delta\hat{F} = \delta\hat{F}^{(\alpha)} + \delta\hat{F}^{(\beta)} + 2\pi\sigma\delta R(t_1) - 2\pi(\kappa_G^{(\alpha)} - \kappa_G^{(\beta)})\sin\psi(t_1)\delta\psi(t_1) \quad . \tag{A7}$$

Here

$$\frac{\delta\hat{F}^{(i)}}{2\pi}=\int_{t_1^{(i)}}^{t_2^{(i)}}dt\left\{\left[\frac{\partial\mathcal{K}^{(i)}}{\partial\psi}-\frac{d}{dt}\frac{\partial\mathcal{K}^{(i)}}{\partial\psi'}\right]\delta\psi+\left[\frac{\partial\mathcal{K}^{(i)}}{\partial R}-\frac{d}{dt}\frac{\partial\mathcal{K}^{(i)}}{\partial R'}\right]\delta R+\frac{\partial\mathcal{K}^{(i)}}{\partial\gamma}\delta\gamma-\frac{d}{dt}\frac{\partial\mathcal{K}^{(i)}}{\partial S'}\delta S\right\}+\frac{\partial\mathcal{K}^{(i)}}{\partial\psi'}\delta\psi\Big|_{t_1^{(i)}}^{t_2^{(i)}}+\frac{\partial\mathcal{K}^{(i)}}{\partial R'}\delta R\Big|_{t_1^{(i)}}^{t_2^{(i)}}+\frac{\partial\mathcal{K}^{(i)}}{\partial S'}\delta S\Big|_{t_1^{(i)}}^{t_2^{(i)}}, \tag{A8}$$

where $t_1^{(i)}$ and $t_2^{(i)}$ are the lower and upper interval boundary of the α and β domain, respectively: $t_1^{(\beta)}=t_0$, $t_2^{(\beta)}=t_1$, $t_1^{(\alpha)}=t_1$, and $t_2^{(\alpha)}=t_2$. The variation $\delta\hat{F}$ can be separated into bulk terms for the α and the β domains and in boundary terms at t_0, t_1, and t_2.

The bulk terms vanish if the Euler-Lagrange equations

$$\frac{\partial\mathcal{K}^{(i)}}{\partial\psi}-\frac{d}{dt}\frac{\partial\mathcal{K}^{(i)}}{\partial\psi'}=0, \tag{A9}$$

$$\frac{\partial\mathcal{K}^{(i)}}{\partial R}-\frac{d}{dt}\frac{\partial\mathcal{K}^{(i)}}{\partial R'}=0, \tag{A10}$$

$$\frac{\partial\mathcal{K}^{(i)}}{\partial\gamma}=0, \tag{A11}$$

$$-\frac{d}{dt}\frac{\partial\mathcal{K}^{(i)}}{\partial S'}=0 \tag{A12}$$

are satisfied in the corresponding intervals $t_1^{(i)}<t<t_2^{(i)}$. Insertion of Eq. (A2) into (A9)–(A12) leads to shape equations, which in the parametrization by the arclength S reads

$$\ddot{\psi}=\frac{\cos\psi\sin\psi}{R^2}-\frac{\dot{\psi}}{R}\cos\psi+\frac{P}{2\kappa^{(i)}}R\cos\psi+\frac{\gamma}{\kappa^{(i)}R}\sin\psi, \tag{A13}$$

$$\dot{\gamma}=\frac{\kappa^{(i)}}{2}(\dot{\psi}-C_0^{(i)})^2-\frac{\kappa^{(i)}\sin^2\psi}{2R^2}+\Sigma^{(i)}+PR\sin\psi, \tag{A14}$$

$$\dot{R}=\cos\psi, \tag{A15}$$

$$\dot{\mathcal{H}}^{(i)}=0. \tag{A16}$$

Here the overdots denote derivatives with respect to S. Equations (A13) and (A14) are the well known shape equations for homogeneous vesicles of spherical topology [42,6]. The functions

$$\mathcal{H}^{(i)}\equiv-\frac{\partial\mathcal{K}^{(i)}}{\partial S'}=\frac{\kappa^{(i)}R}{2}\left\{\left(\frac{\psi'}{S'}\right)^2-\left(\frac{\sin\psi}{R}-C_0^{(i)}\right)^2\right\}-\Sigma^{(i)}R-\frac{P}{2}R^2\sin\psi+\gamma\cos\psi \tag{A17}$$

play the role of Hamiltonian functions, which are conserved according to (A14). The function $Z(S)$ is determined by the geometrical relation $\dot{Z}+\sin\psi=0$.

The condition $\delta\hat{F}=0$ for variations $\delta S(t_1)\neq0$, and $\delta S(t_2)\neq0$, together with (A14), leads to the conditions

$$\mathcal{H}^{(\alpha)}=\mathcal{H}^{(\beta)}=0\quad. \tag{A18}$$

The geometric conditions $R(S_0)=R(S_2)=0$, $\psi(S_0)=0$, and $\psi(S_2)=\pi$, together with (A18), fix the boundary conditions $\gamma(S_0)=\gamma(S_2)=0$.

Stationarity of $\hat{F}$ with respect to variations $\delta R(t_1)\neq0$ and $\delta\psi(t_1)\neq0$, together with (A7) and (A8), leads to the conditions

$$\left.\frac{\partial\mathcal{K}^{(\alpha)}}{\partial\psi'}\right|_{t=t_1+\epsilon}-\left.\frac{\partial\mathcal{K}^{(\beta)}}{\partial\psi'}\right|_{t=t_1-\epsilon}=[\kappa_G^{(\beta)}-\kappa_G^{(\alpha)}]\sin\psi(t_1), \tag{A19}$$

$$\left.\frac{\partial\mathcal{K}^{(\alpha)}}{\partial R'}\right|_{t=t_1+\epsilon}-\left.\frac{\partial\mathcal{K}^{(\beta)}}{\partial R'}\right|_{t=t_1-\epsilon}=\sigma \tag{A20}$$

at $t=t_1$. After reparametrization with the arclength S one obtains from (A19) and (A20) the matching conditions

$$\gamma(S_1+\epsilon)-\gamma(S_1-\epsilon)=\sigma, \tag{A21}$$

$$\kappa^{(\alpha)}\dot{\psi}(S_1+\epsilon)-\kappa^{(\beta)}\dot{\psi}(S_1-\epsilon)=(\kappa^{(\beta)}-\kappa^{(\alpha)}+\kappa_G^{(\beta)}-\kappa_G^{(\alpha)})\frac{\sin\psi(S_1)}{R(S_1)}+\kappa^{(\alpha)}C_0^{(\alpha)}-\kappa^{(\beta)}C_0^{(\beta)} \tag{A22}$$

at $S=S_1$. Here the continuity of $R(S)$ and $\psi(S)$ has been assumed. [If, for example, one allows the shape to have a "kink" with $\psi(S_1-\epsilon)-\psi(S_1+\epsilon)\neq0$, $\delta\psi(t_1-\epsilon)$ and $\delta\psi(t_1+\epsilon)$ have to be varied independently. The matching condition (A19) is in this case replaced by two independent boundary conditions $\partial\mathcal{K}^{(\beta)}/\partial\psi'=\kappa_G^{(\beta)}\sin\psi(t_1-\epsilon)$ and $\partial\mathcal{K}^{(\alpha)}/\partial\psi'=\kappa_G^{(\alpha)}\sin\psi(t_1+\epsilon)$ at $t=t_1\mp\epsilon$.] For a homogeneous membrane with $\sigma=0$, $\kappa^{(\alpha)}=\kappa^{(\beta)}$, $\kappa_G^{(\alpha)}=\kappa_G^{(\beta)}$, and $C_0^{(\alpha)}=C_0^{(\beta)}$, Eqs. (A21) and (A22) reduce to continuity conditions for $\dot{\psi}$ and γ at $S=S_1$.

The shape of a vesicle with two domains can be determined as a solution of the shape equations (A13)–(A16) together with the matching conditions (A21) and (A22). This method can be generalized for an axisymmetric vesicle with three domains. For more than three domains, the assumption of axisymmetry can no longer be justified.

APPENDIX B: THE GENERAL NECK CONDITION

The generalized neck condition that describes the limit shapes L_{CB} can be discussed in the context of a simple toy model introduced by Fourcade *et al.* [44]. In this model, the nearly vesiculated shape is approximated by a variational contour, which consists of four parts I–IV; see Fig. 13. The parts I and IV are hemispheres of radii

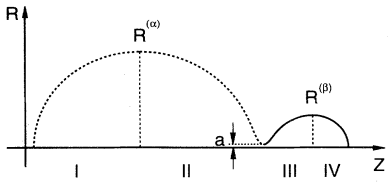

FIG. 13. Simple toy model for vesiculated shapes. The shape consists of four parts I–IV. Parts I and II form domain α, III and IV form domain β. Parts I and IV are hemispheres of radii $R^{(\alpha)}$ and $R^{(\beta)}$, respectively. Parts II and III form the neck region with neck diameter a.

$R^{(i)}$, described by $\sin\psi = R/R^{(i)}$, where $i = \alpha, \beta$. The neck region is formed by the parts II and III, where

$$\sin\psi = \frac{R}{R^{(i)}+a} + \frac{R^{(i)}a}{R(R^{(i)}+a)} \tag{B1}$$

and a denotes the neck diameter. The two domains are separated by a domain boundary located within the neck where $R = a$.

For small a, the surface areas $A^{(\alpha)}$ and $A^{(\beta)}$ of the domains can be expanded as

$$A^{(i)} = 4\pi(R^{(i)})^2 + 2\pi R^{(i)}a - \pi a^2 \ln\frac{a}{R^{(i)}} + O(a^2) \quad . \tag{B2}$$

The enclosed volume can be expressed as $V = V^{(\alpha)} + V^{(\beta)}$ with

$$V^{(i)} = \frac{4}{3}\pi(R^{(i)})^3 + \pi(R^{(i)})^2 a + O(a^2) \quad . \tag{B3}$$

The total energy

$$F = F_b + 2\pi\sigma a + PV \tag{B4}$$

of this shape can be expressed as a function of the neck diameter a for fixed areas $A^{(\alpha)}$ and $A^{(\beta)}$. Within this toy model, only two parameters $R^{(\alpha)}$ and $R^{(\beta)}$ are available to take into account the constraints. Here both parameters are used to fix the areas $A^{(\alpha)}$ and $A^{(\beta)}$. Therefore, the enclosed volume cannot be fixed at the same time and the pressure ensemble is used. In order to fix the areas $A^{(i)}$, the radii $R^{(i)}$ of the limit spheres obey

$$R^{(i)}(a) = R_0^{(i)} - \frac{a}{4} - \frac{a^2}{8R_0^{(i)}}\ln\frac{a}{R_0^{(i)}} + O(a^2) \quad , \tag{B5}$$

where $R_0^{(i)}$ denote the radii of the spheres that form the limit shape for $a = 0$. Inserting Eq. (B5) into (B2) and (B3), the energy F reads

$$F = 2\pi\kappa^{(\alpha)}(R_0^{(\alpha)})^2\left(\frac{2}{R_0^{(\alpha)}} - C_0^{(\alpha)}\right)^2 + 2\pi\kappa^{(\beta)}(R_0^{(\beta)})^2\left(\frac{2}{R_0^{(\beta)}} - C_0^{(\beta)}\right)^2$$
$$-4\pi\left[\frac{\kappa^{(\alpha)}}{R_0^{(\alpha)}} + \frac{\kappa^{(\beta)}}{R_0^{(\beta)}} - \frac{1}{2}\kappa^{(\alpha)}C_0^{(\alpha)} - \frac{1}{2}\kappa^{(\beta)}C_0^{(\beta)} - \frac{1}{2}\sigma\right]a + O(a^2\ln a) \; . \tag{B6}$$

The vesiculated shape with $a = 0$ is stationary with respect to variations of the neck diameter a if

$$\frac{\kappa^{(\alpha)}}{R_0^{(\alpha)}} + \frac{\kappa^{(\beta)}}{R_0^{(\beta)}} = \frac{1}{2}\left(\kappa^{(\alpha)}C_0^{(\alpha)} + \kappa^{(\beta)}C_0^{(\beta)} + \sigma\right) \quad . \tag{B7}$$

This condition is equivalent to (15).

APPENDIX C: NONSPHERICAL LIMIT SHAPES

Limit shapes L_{CB} for $P = 0$ consist of two spheres, connected by an infinitesimal neck. For these shapes, the general neck condition leads to the exact expression (16) for the line $\lambda_L(x)$ in the phase diagrams.

The limit shapes L_{CB} that occur for fixed reduced volume consist of a sphere and a homogeneous spherical prolate. For such a shape, λ_L can be expressed as

$$\lambda_L(x,v) = \frac{\kappa^{(\alpha)}}{\kappa^{(\beta)}}\frac{2M_0[\tilde{v}_P(x,v)]R_P}{(1-x)^{1/2}} + \frac{2}{x^{1/2}}$$
$$-\frac{\kappa^{(\alpha)}}{\kappa^{(\beta)}}c_0^{(\alpha)} - c_0^{(\beta)} . \tag{C1}$$

Here

$$\tilde{v}_P(x,v) = \frac{v - x^{3/2}}{(1-x)^{3/2}} \tag{C2}$$

is the reduced volume of the prolate introduced in Sec. III B, $M_0(\tilde{v}_P)$ is the mean curvature at the pole of the prolate with reduced volume $\tilde{v}_P$, and surface area $A = 4\pi R_P^2$. The function $M_0(v_P)$ can be easily obtained by solving shape equations for homogeneous shapes. The lines L_{CB} shown in Figs. 7 and 9 have been obtained using Eq. (C1)

[1] R. Lipowsky, Nature **349**, 475 (1991).
[2] K. Berndl, J. Käs, R. Lipowsky, E. Sackmann, and U. Seifert, Europhys. Lett. **13**, 659 (1990).
[3] J. Käs and E. Sackmann, Biophys. J. **60**, 825 (1991).
[4] E. Evans and W. Rawicz, Phys. Rev. Lett. **64**, 2094 (1990).
[5] W. Wiese, W. Harbich, and W. Helfrich, J. Phys. Condens. Matter **4**, 1647 (1992).
[6] U. Seifert, K. Berndl, and R. Lipowsky, Phys. Rev. A **44**, 1182 (1991).
[7] L. Miao, B. Fourcade, M. Rao, M. Wortis, and R. K. P. Zia, Phys. Rev. A **43**, 6843 (1991).
[8] W. Helfrich, Z. Naturforsch. Teil C **28**, 693 (1973).
[9] U. Seifert, Phys. Rev. Lett. **66**, 2404 (1991).
[10] F. Jülicher, U. Seifert, and R. Lipowsky, J. Phys. (France) II **3**, 1681 (1993).
[11] F. Jülicher, U. Seifert, and R. Lipowsky, Phys. Rev. Lett. **71**, 452 (1993).
[12] E. Farge and P. Devaux, Biophys. J. **61**, 347 (1992).
[13] H.-G. Döbereiner, J. Käs, D. Noppl, I. Sprenger, and E. Sackmann, Biophys. J. **65**, 1396 (1993).
[14] M. Mutz and D. Bensimon, Phys. Rev. A **43**, 4525 (1991).
[15] B. Fourcade, M. Mutz, and D. Bensimon, Phys. Rev. Lett. **68**, 2551 (1992).
[16] X. Michalet, D. Bensimon, and B. Fourcade, Phys. Rev. Lett. **72**, 168 (1994).
[17] C. Gebhardt, H. Gruler, and E. Sackmann, Z. Naturforsch. Teil C **32**, 581 (1977).
[18] *The Structure and Dynamics of Membranes*, Handbook of Biological Physics Vol. 1, edited by R. Lipowsky and E. Sackmann (Elsevier, Amsterdam, 1995).
[19] M. Bloom, E. Evans, and O. Mouritsen, Q. Rev. Biophys. **24**, 293 (1991).
[20] P. Rice and H. McConnell, Proc. Natl. Acad. Sci. U.S.A. **86**, 6445 (1989).
[21] D. Benvegnu and H. McConnell, J. Phys. Chem. **96**, 6820 (1992).
[22] R. D. H. McConnell, J. Phys. Chem. **98**, 5389 (1994).
[23] S.-W. Wu and H. McConnell, Biochemistry **14**, 847 (1975).
[24] D. J. Recktenwald and H. McConnell, Biochemistry **20**, 4505 (1981).
[25] M. Vist and J. Davis, Biochemistry **29**, 451 (1990).
[26] P. Almeida, W. Vaz, and T. Thompson, Biochemistry **31**, 6739 (1992).
[27] P. Yeagle, *Biology of Cholesterol* (Chemical Rubber, Boca Raton, FL, 1988).
[28] M. Bretscher and S. Munro, Science **261**, 1280 (1993).
[29] R. Lipowsky, Curr. Opinion Struct. Biol. **5**, 531 (1995).
[30] V. Markin, Biophys. J. **36**, 1 (1981).
[31] S. Leibler, J. Phys. (Paris) **47**, 507 (1986).
[32] S. Leibler and D. Andelman, J. Phys. **48**, 2013 (1987).
[33] U. Seifert, Phys. Rev. Lett. **70**, 1335 (1993).
[34] R. Lipowsky, J. Phys. (France) II **2**, 1825 (1992).
[35] R. Lipowsky, Biophys. J. **64**, 1133 (1993).
[36] D. Andelman, T. Kawakatsu, and K. Kawasaki, Europhys. Lett. **19**, 57 (1992).
[37] T. Kawakatsu, D. Andelman, K. Kawasaki, and K. Taniguchi, J. Phys. (France) II **3**, 971 (1993).
[38] F. Jülicher and R. Lipowsky, Phys. Rev. Lett. **70**, 2964 (1993).
[39] T. Taniguchi, K. Kawasaki, D. Andelman, and T. Kawakatsu, J. Phys. (France) II **4**, 1333 (1994).
[40] F. MacKintosh, Phys. Rev. E **50**, 2891 (1994).
[41] J. Harden and F. MacKintosh, Europhys. Lett. **28**, 495 (1994).
[42] H. Deuling and W. Helfrich, J. Phys. **37**, 1335 (1976).
[43] S. Svetina and B. Zeks, Eur. Biophys. J. **17**, 101 (1989).
[44] B. Fourcade *et al.*, Phys. Rev. E **49**, 5276 (1994).
[45] M. do Carmo, *Differential Geometry of Curves and Surfaces* (Prentice-Hall, Englewood Cliffs, NJ, 1976).
[46] U. Seifert, L. Miao, H.-G. Döbereiner, and M. Wortis, in *The Structure and Conformation of Amphiphilic Membranes*, edited by R. Lipowsky, D. Richter, and K. Kremer, Springer Proceedings in Physics Vol. 66 (Springer, Berlin, 1991), pp. 93–96.
[47] H. Duwe, J. Käs, and E. Sackmann, J. Phys. (Paris) **51**, 945 (1990).
[48] M. Glaser, Curr. Opinion Struct. Biol. **3**, 475 (1993).